

## Changes in the titanium oxide optical properties during crystallization

© S.V. Bulyarskiy<sup>1</sup>, D.A. Koiva<sup>1</sup>, G.G. Gusarov<sup>1</sup>, V.V. Svetukhin<sup>2</sup>

<sup>1</sup>Institute of Nanotechnology of Microelectronics, Russian Academy of Sciences, Moscow, Russia

<sup>2</sup>Scientific-Manufacturing Complex „Technological Centre“, Zelenograd, Moscow, Russia

e-mail: bulyar2954@mail.ru

Received on June 11, 2021

Revised on July 16, 2021

Accepted on July 28, 2021

Crystallization of amorphous titanium oxide films synthesized by magnetron sputtering was carried out at temperatures of 700, 800, and 900°C in an oxygen atmosphere. The refractive index of the films increases during crystallization with a time constant that depends on temperature, which made it possible to determine the activation energy of the crystallization process on the order of 0.6 eV. The growth kinetics model for the titanium oxide nanocrystals, which is used in this work, showed that the indicated activation energy corresponds to the diffusion energy of oxygen vacancies. This process is decisive for the growth of titanium oxide nanocrystals upon annealing in an oxygen atmosphere. The study of photoluminescence has shown that crystallization leads to a change in the ratio of intensities of different emission bands. The bands that are associated with the oxygen vacancy are extinguished. A decrease in the concentration of these vacancies in films leads to an increase in their resistance and stabilization of the films in time.

**Keywords:** titanium oxide films, crystallization, refractive index, photoluminescence.

DOI: 10.21883/EOS.2022.14.54001.2428-21

### Introduction

Thin films of titanium oxide find important application in the creation of active elements of nanoelectronics, including the manufacture of CMOS gates [1,2], gas sensors [3], and solar cells with a TiO<sub>2</sub> heterojunction [4,5]. The TiO<sub>2</sub>/silicon heterojunction has a large break in the potential curves in the valence band, which creates a potential barrier for holes at about 2.0 eV in this case, and blocks the transport of holes into silicon thus increasing the efficiency of photodetectors. These products require stable thin films with high resistance. It is known that the refraction index of titanium oxide increases after annealing, while the forbidden band width slightly decreases [6,7]. Structural defects determine the electronic parameters of these active elements in all cases, which makes it necessary to study in detail the mechanisms for their number control.

Titanium oxide films are often created by magnetron sputtering for the production of nanoelectronic elements [8–10]. The structure of such films is amorphous immediately after synthesis [11]. Crystallization of thin films begins at temperatures above 700°C if they are annealed in an oxygen atmosphere or in air [12,13]. Such annealing of titanium oxide changes the phase composition, morphological structure, and defects content. In order to effectively use films in nanoelectronics, it is necessary to understand the mechanisms of crystallization and film evolution from amorphous to nanocrystalline.

Analysis of the defect formation processes in titanium oxide is carried out, as a rule, by experimental study of emission bands after films treatment under various conditions [14–24]. Oxygen vacancies determine the fluorescence

in the visible region of the spectrum with the energy of the band maximum 2.4 eV [16–18]. To explain the origin of this band, a donor-acceptor mechanism of photoluminescence in TiO<sub>2</sub> nanostructures was proposed, under which singly ionized oxygen vacancies capture photogenerated electrons, while surface hydroxyl groups capture formed holes [20]. The band with the emission maximum in the 1.2 eV region in the 1.4 eV region is due to interstitial titanium ions Ti<sup>4+</sup>. Defect states associated with interstitial titanium ions contribute to the near-IR luminescence [24]. The broad luminescence band 1.27 eV is associated with Ti<sub>i</sub><sup>3+</sup> defect on the surface of the nanocrystal, while the 1.47 eV band is attributed to interstitial Ti<sup>4+</sup> in its bulk. The results of X-ray photoelectron spectroscopy confirm the presence of both Ti<sub>i</sub><sup>3+</sup>- and Ti<sub>i</sub><sup>4+</sup>-defects in the films, and the dependence of their content on treatment. In the paper [21] it was assumed that the photoluminescence band (2.4 eV) in TiO<sub>2</sub> is associated with the recombination of free electrons with holes that are captured in traps, and the red band (2.05 eV) can be associated with complexes of interstitial titanium and oxygen vacancies. It has been shown that in both anatase and rutile the weakly bound self-trapped excitons actually consist of polarons and provide broad emission bands in the visible region of the spectrum. This is the reason for the P5 2.85 eV band, which is produced by self-trapped excitons [18,21].

Thus, the optical, photoluminescent properties, and the content of defects in thin films of titanium oxide are determined both by the conditions of production, and by subsequent technological treatments. In this paper we study the optical and photoluminescent properties of thin films of titanium oxide, which were annealed in oxygen

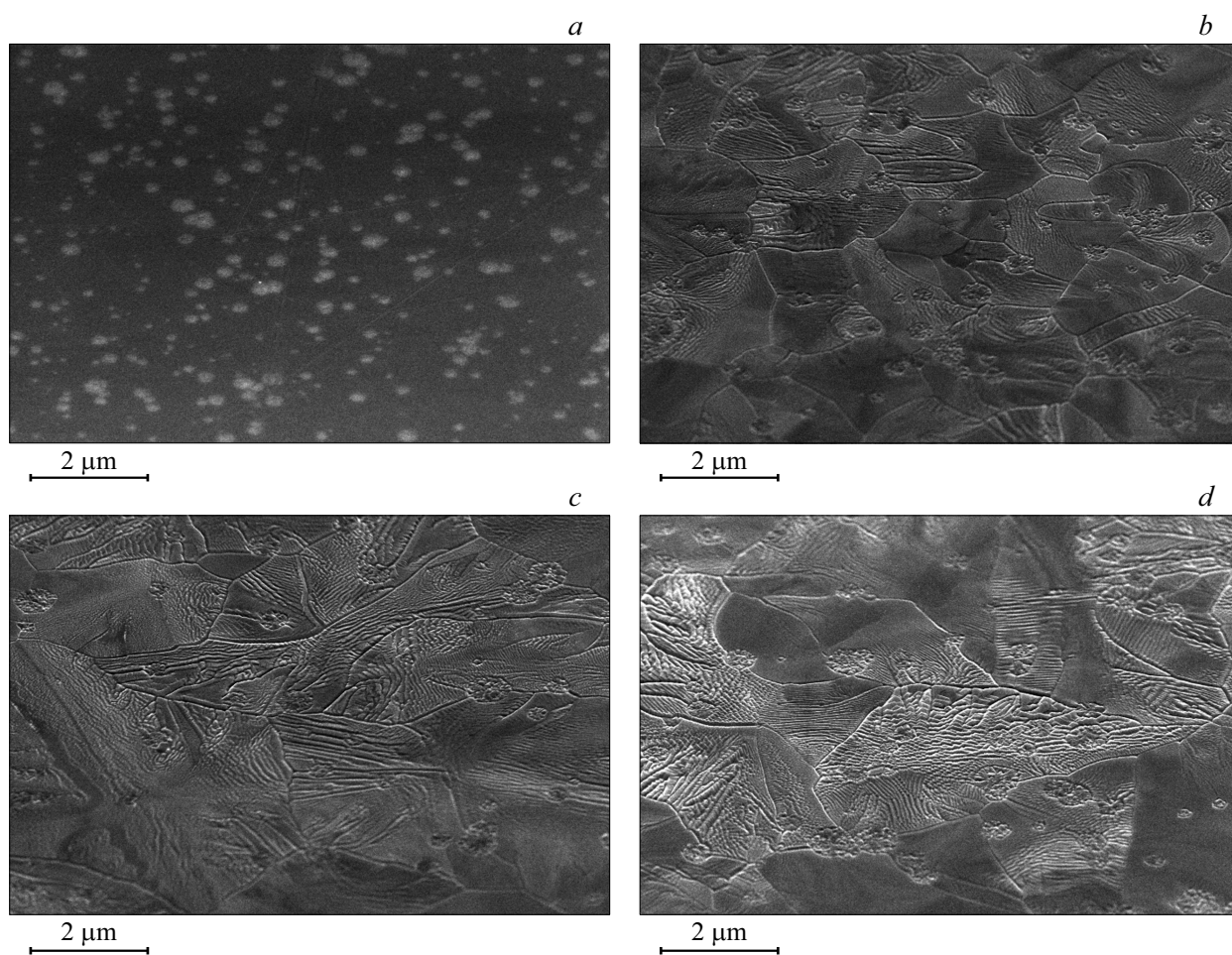


**Figure 1.** Images of the film surface of  $\text{TiO}_x$  samples immediately after synthesis (*a*) and after annealing at temperature of  $900^\circ\text{C}$  for 10 min (*b*) and 20 min (*c*) in a pulse annealing unit and 120 min (*d*) in a tube furnace.

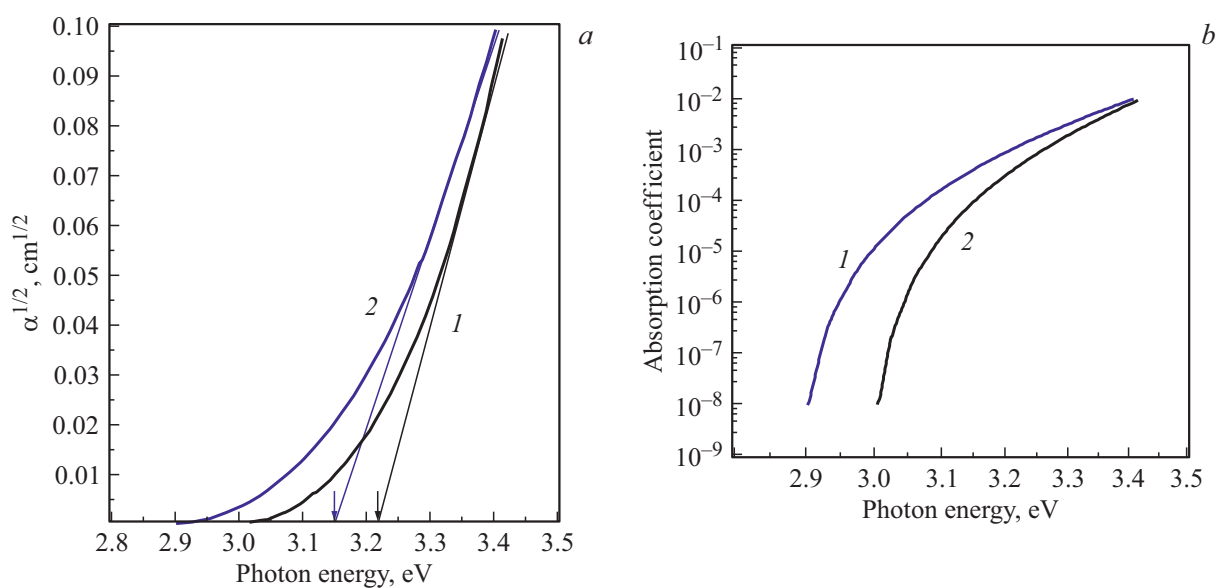


**Figure 2.** Absorption spectra immediately after synthesis (curve *1*) and after annealing in oxygen atmosphere at temperature of  $900^\circ\text{C}$  for 1 h (curve *2*). (*a*) Determination of forbidden band gap; (*b*) Urbach edge.

atmosphere for different times and at different temperatures. The behavior of the optical properties of these films during annealing in the oxygen atmosphere is studied in order to obtain stable layers with low electrical conductivity, which is achieved by reducing the concentration of oxygen vacancies.

## Synthesis and heat treatment of films

TiO<sub>x</sub> titanium oxide films were synthesized by magnetron sputtering of the titanium target in argon and oxygen atmosphere on thermally oxidized n-type single-crystal silicon wafers. The working gases supply to the chamber was carried out using two automatic regulators. The flow of Ar was 20 cm<sup>3</sup>/min, of O<sub>2</sub> — 4.7 cm<sup>3</sup>/min. The power of the magnetron during the gas discharge was 300 W, and the sputtering time was 3 h.

The films were annealed in the oxygen atmosphere at temperatures of 900, 800, and 700°C; the annealing time was varied in order to track the kinetics of crystallization processes.

## Morphological and phase analysis of TiO<sub>x</sub> before and after annealing

Morphological analysis was carried out using a scanning electron microscope. Sample images are shown in Fig. 1.

The surface of the initial samples immediately after synthesis was fine-grain with individual coarse inclusions (Fig. 1, *a*). After annealing, the surface became denser, and the development of large-block structures with clear boundaries of individual blocks became noticeable, however, transmission electron microscopy showed that the blocks also consist of nanocrystals with sizes from 20 to 40 nm.

X-ray phase analysis showed that the films immediately after sputtering were X-ray amorphous. After annealing at temperature of 900°C for 1 h the titanium oxide films begin to crystallize. In this case, the X-ray amorphous phase partially transforms into anatase, and the samples become two-phase one. The Auger analysis revealed that the films have TiO<sub>x</sub> composition, which is uniform throughout the entire film thickness. The Ti/O ratio after annealing was close to 0.5; therefore, the films became almost stoichiometric.

Electrical measurements have demonstrated the high resistivity of the films after annealing.

## Experimental study of the optical properties of titanium oxide films during crystallization

The components of the imaginary refraction index were determined on SENDURO spectral ellipsometer (SENTECH Instruments GmbH) with the SpectraRay/3 mathematical processing package. The absorption coefficient was

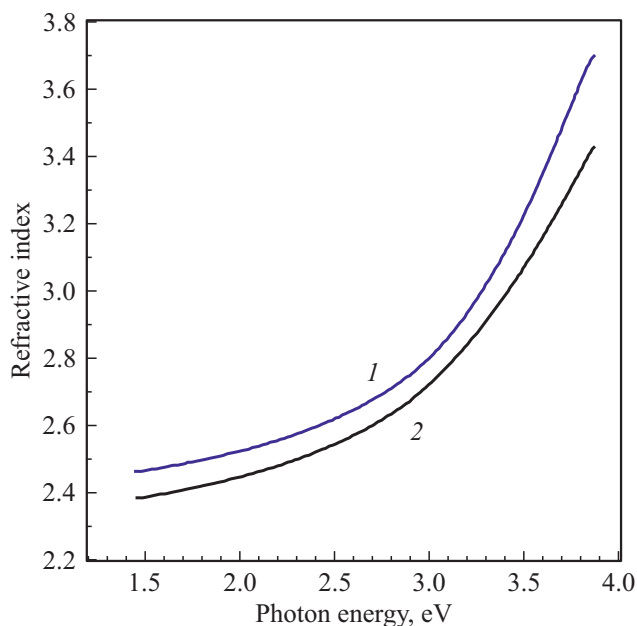


**Figure 3.** Refraction index spectra immediately after synthesis (curve 1) and after annealing in oxygen atmosphere at temperature of 900°C for 1 h (curve 2).

calculated from the extinction coefficient by the formula:

$$\alpha = \frac{4\pi k}{\lambda}, \quad (1)$$

where,  $k$  is the extinction coefficient, and  $\lambda$  is the wavelength.

The spectral change in the absorption index is shown in Fig. 2. The absorption spectrum as a whole corresponds to the assumption of indirect optical transitions of titanium oxide [6,7], however, it has a feature associated with the presence of X-ray amorphous phase, which manifests itself in the presence of Urbach edge (Fig. 2, *b*), the appearance of which is associated with the density of states below the bottom of the conduction band. Crystallization processes during annealing result in ordering of the films, their band width decreases from 3.22 to 3.14 eV, which corresponds to the result of X-ray phase analysis, which showed the presence of anatase nanocrystals in the films (Fig. 2, *a*).

The refraction index spectra of the samples before and after annealing are shown in Fig. 3. After annealing in the oxygen atmosphere at a temperature of 900°C for 1 h, the absorbance of the samples increases, and their refraction index increases throughout the entire spectral region.

The drop in the value of the refraction index with the photon energy of the incident light decreasing indicates the normal dispersion of the samples (Fig. 3). The measurement results show that the refraction index increases during annealing from 2.42 to 2.53 at He-Ne laser wavelength of 633 nm, and reaches a value close to the refraction index of TiO<sub>2</sub> bulk anatase. It was noted in the [6] that the films synthesized by the sol-gel method are amorphous

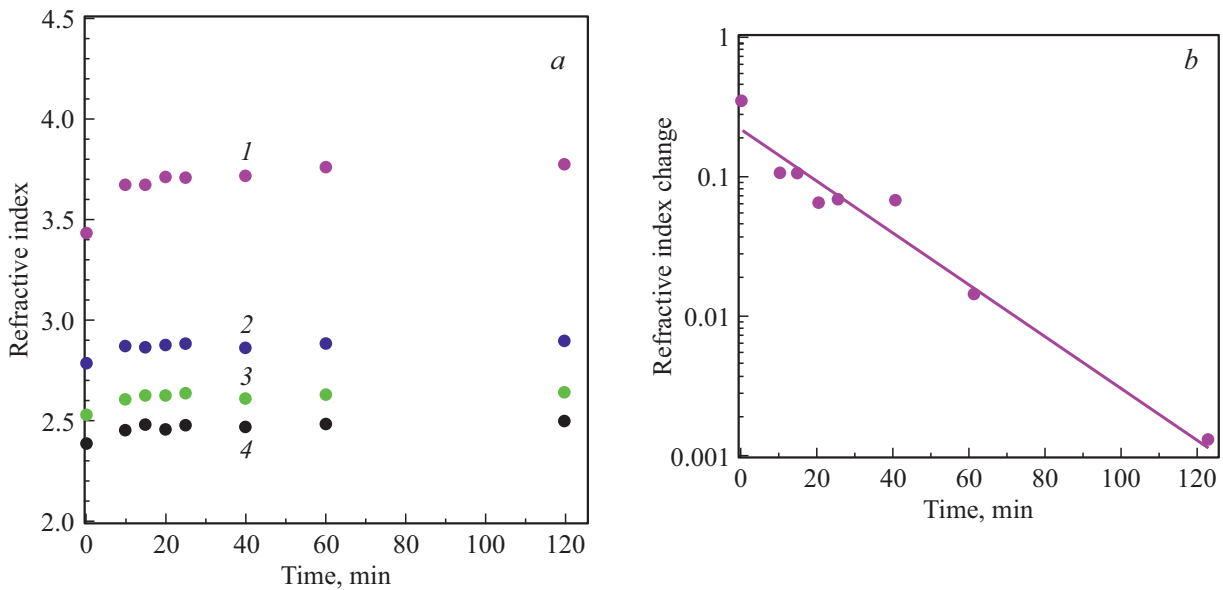


**Figure 4.** Kinetics of the refraction index change of thin films of titanium oxide during annealing at 900°C. (a) Kinetics of the index change measured at different wavelengths, nm: 1 — 321, 2 — 400, 3 — 500, 4 — 850 nm; (b) kinetics of the increment change of the refraction index during the annealing time at wavelength of 321 nm.

immediately after preparation, and their refraction index is 1.96 at 633 nm. In our case, films synthesized by magnetron sputtering have the refraction index of 2.42. These films are X-ray amorphous, but fine crystalline with nanocrystal sizes less than 5 nm. Therefore, their refraction index is higher. Upon annealing at 900°C, the refraction index increasing may be due to the thermal growth of grains, which increases the packing density. Both of these results show that during annealing the processes of crystallization of small particles into larger nanoparticles take place. Thus, the process of growth of nanocrystals and the merging of fine crystalline nuclei, similar to the process of coalescence of substance clusters, is observed.

Titanium oxide films were annealed in the oxygen atmosphere at various temperatures. Annealing at each temperature was performed during different time period, which made it possible to study the kinetics of the refraction index change during film crystallization. The measurement results are presented in Fig. 4.

The refraction index change with annealing time can be described by the empirical formula:

$$\Delta n = \Delta n_{\infty} [1 - \exp(-t/\tau)], \quad (2)$$

where  $\Delta n_{\infty}$  is the maximum change in the annealing index at the end of the crystallization process,  $t$  is the annealing time,  $\tau$  is the crystallization time constant.

The kinetics of the crystallization process makes it possible to determine the time constant of this process ( $\tau$ ), this can be done at different annealing temperatures. The time constant was the same when calculated at different wavelengths. Its value did not depend on the wavelength, but depended on the temperature. It increases while the

temperature decreases. The reciprocal of the time constant of the crystallization process was plotted in Arrhenius coordinates (Fig. 5), which makes it possible to calculate the crystallization energy of titanium oxide. The result of the calculation gives the value  $0.6 \pm 0.1$  eV.

The results of X-ray phase analysis and the optical properties of the films show that they tend to crystallize in the anatase structure during annealing in the oxygen atmosphere. The crystallization process has an activation energy of about 0.6 eV.

## Photoluminescence of thin films

The photoluminescence of the films was excited by a laser with a wavelength of 325 nm. The photoluminescence spectra of titanium oxide immediately after synthesis and after annealing at temperature of 900°C for 1 h are shown in Fig. 6.

The results of the luminescence study show that before and after annealing the energy of the maximum of the emission band changes insignificantly. This change may be associated with a width change in the forbidden band gap of the material after annealing. This fact allows us to assume the stability of the mechanisms that determine the emission of these bands. The dispersion of emission bands depends both on the disorder in the amorphous material and on the magnitude of the electron-phonon interaction. The dispersion decreases for all bands during annealing in the oxygen atmosphere. This is due to the fact that annealing is accompanied by the material crystallization, and the component of the dispersion, which is associated with amorphization, decreases significantly. However, the

Parameters for separating photoluminescence spectra into components

Number of radiation band (Fig. 6)	1		2		3		4		5	
	$E_1$	$\sigma$ ,	$E_2$	$\sigma$ ,	$E_3$	$\sigma$	$E_4$	$\sigma$	$E_5$	$\sigma$
Immediately after synthesis	1.18	0.07	1.48	0.10	1.96	0.11	2.40	0.13	2.8	0.11
After annealing in oxygen at 900°C 1 h	1.22	0.052	1.44	0.08	1.98	0.10	2.42	0.11	2.86	0.10

Note.  $E_i$  is energy of emission band maximum,  $\sigma$  is dispersion of emission band.

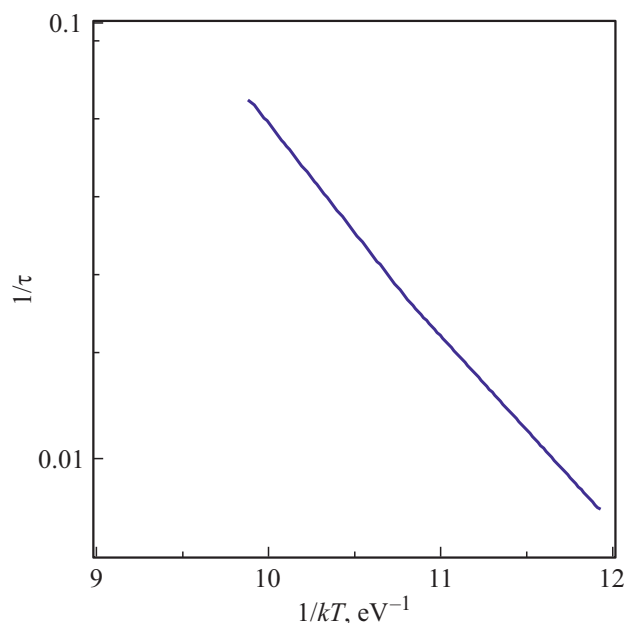


**Figure 5.** Inverse constant of the crystallization process vs temperature in Arrhenius coordinates.

dispersion of emission bands in the crystalline material remains significant, which indicates the leading role of the electron-phonon interaction in the formation of emission bands in titanium oxide. The effect of the electron-phonon interaction on radiation in oxide materials was noted in previous works. The paper [14] is one of the first, where the temperature dependences of the luminescence of titanium dioxide in the anatase and rutile phases are studied in detail, and the conclusion is made about the significant role of the electron-phonon interaction in the formation of emission spectra. The authors of the paper [15] showed that the band 1.22 eV in crystalline  $\text{TiO}_2$  is related to the interstitial titanium complex and is due to strong electron-phonon interaction. In this paper a method for plotting the configuration-coordinate diagrams based on the measured emission bands is developed.

Annealing at high temperatures in the oxygen atmosphere leads to two parallel processes: first, oxygen interacts with oxygen vacancies, and their concentration on the surface

decreases. A vacancy concentration gradient occurs, and this is the reason for the movement of oxygen vacancies to the surface, while the surface is enriched with titanium atoms in the lack of oxygen. Secondly, titanium atoms on the surface interact with the oxygen of the reactor, and titanium oxide is formed, which completes the crystal lattice of the already existing titanium oxide nanoparticles, which increase in size, and this is observed experimentally, including by the method of transmission electron microscopy. The tendency to multiple amplification of the emission bands (Fig. 6) after annealing in oxygen is primarily due to the material crystallization, which leads to its ordering, thus reducing the losses due to nonradiative recombination. However, annealing affects each of the bands differently. The intensity of the emission bands, which are associated with the electronic states of defects, change not only due to the ordering of the material structure, but also as a result of change in the defects concentration. The intensity of the band 1 associated with interstitial titanium ions  $\text{Ti}^{+3}$  on the surface of nanocrystals increases by 168 times, and the intensity of the band 4 associated with oxygen vacancies increases by 110 times. This shows a tendency towards the concentration decreasing of oxygen vacancies, but they do not disappear. As shown by the results of high-resolution transmission electron microscopy, the nanocrystals remain small with sizes of about 20–40 nm and are surrounded by the amorphous phase, which is consistent with the presence of the Urbach edge in the absorption spectra (Fig. 2, b). Therefore, there are many oxygen vacancies. The intensity of the band 3 becomes relatively less, this is due to the fact that the number of interstitial titanium ions  $\text{Ti}^{+4}$  in the bulk of nanocrystals decreases. The intensity of the band 3, which is associated with complexes of interstitial titanium and oxygen vacancies, noticeably decreases, which indicates that vacancies from the bulk of nanocrystals are transferred to their surface.

Thus, the crystallization process is accompanied by the vacancies movement from the bulk of growing nanocrystals to their surface.

### Kinetic model of titanium oxide crystallization

We previously considered models of the processes of nanocrystals formation during annealing in the papers [25,26]. Films of titanium oxide immediately after synthesis by the magnetron method are X-ray amorphous and consist of nanocrystals smaller than 5 nm, which can be considered as crystallization centers. Annealing of titanium oxide leads to self-organization of atoms and causes the following transformation: crystallization centers combine into clusters; the clusters become denser and turn into small nanocrystals. Then small nanocrystals continue to grow, ordering occurs inside them, and larger nanocrystals appear [25,26]. This stage was called coalescence.

There are two models of nanocrystal growth: homogeneous and heterogeneous. The homogeneous formation of clusters corresponds to the scheme:  $A_i + A \leftrightarrow A_{i+1}$ . This model is only suitable for the growth of crystals that consist of only one kind of atom, such as silicon [25,26]. Titanium oxide consists of titanium and oxygen atoms; therefore, the growth of its crystals occurs according to a heterogeneous mechanism. The heterogeneous growth of the nanocrystal is described using the following equation:  $A_iC + A \leftrightarrow A_{i+1}C$  Initially, the titanium oxide film consists of crystallization centers less than 5 nm in size. There are many broken bonds and vacancies on the surface of these centers. The film is annealed in the oxygen atmosphere. The oxygen interaction with nanocrystals is carried out on the surface of these single crystals. Therefore, their surface is depleted of oxygen vacancies. There is a diffusion flow of oxygen vacancies to the surface of nanocrystals, and the surface is enriched with titanium ions  $Ti^{+3}$ . These ions react with oxygen to form titanium oxide, which finish the lattice and increase the size of the existing oxide nanoparticles. The process of oxygen vacancies movement to the surface is decisive, so, finally, it causes the size of nanocrystals increasing. This process can be considered as the escape of oxygen vacancies to sinks, which include the boundaries of growing single crystals. Crystallization centers capture oxygen atoms to form oxide particles and emit oxygen vacancies (monomers). This process is described using the system of equations [25,26]:

$$\begin{cases} \frac{dN_i}{dt} = -N_i(k_iN + g_i) + g_{i+1}N_{i+1} + k_{i-1}NN_{i-1}, \\ \frac{dN}{dt} = -N \sum_{i=0} k_iN_i + \sum_{i=1} g_iN_i, \end{cases} \quad (3)$$

$$N_C = \sum_{i=0} N_i(t) = \text{const},$$

where  $N_i$  is the bulk-average concentration of crystallization centers that attached  $i$  particles;  $N$  is concentration of monomers (oxygen vacancies);  $k_iN$  and  $g_i$  are capture and ejection rates of the monomer for the crystallization center that attached  $i$  particles.

Increasing of the size of crystallization centers (formula (3)) as a result of diffusion of oxygen vacancies to

sinks occurs at the initial stage of the process [25,26], when a fractal cluster is formed from nucleation centers that were formed during synthesis, then the cluster continues to compact as before due to the escape of oxygen vacancies to the sinks, the growth of the nanocrystal occurs. The growth of the nanocrystal is called reactionary (formula (3)) if there is a potential barrier at the boundary of the nucleation center. In this case, the vacancy escape from the surface of the crystallization center requires energy associated with overcoming the potential barrier. For kinetic coefficients, you can use the expressions [27]:

$$k_i = \begin{cases} k_D = 4\pi Db, \\ k_R = \frac{4\pi b^2 D}{r_0} \exp\left\{-\frac{E_i}{kT}\right\}, \end{cases} \quad (4)$$

where  $k_D$  is the probability of oxygen vacancy escape to the surface of growing nanocrystal under the diffusion mechanism of its formation;  $k_R$  is the probability of vacancy escape from the crystallization center, if it is necessary to overcome the potential barrier, which corresponds to the reaction mechanism of nanocrystal growth;  $D$  is diffusion coefficient of the oxygen vacancy in a substance;  $b$  is lattice period of a growing nanocrystal;  $r_0$  is nanocrystal radius.

The concentration of crystallization centers was formed during the synthesis and does not change with time. Therefore, we can find the exact solution (3) in the following form:

$$t = C + {}_2F_1\left(\alpha, \alpha, 1 + \alpha, -\frac{N(0) + N_C - N_E}{N_E - N}\right) \times \left(\frac{N_C}{N_E - N}\right)^\alpha \frac{1}{k_D N_C}, \quad (5)$$

where the constant is defined by the equation

$$C = -{}_2F_1\left(\alpha, \alpha, 1 + \alpha, -\frac{N(0) + N_C - N_E}{N_E - N(0)}\right) \times \left(\frac{N_C}{N_E - N(0)}\right)^\alpha \frac{1}{k_D N_C}.$$

Here  ${}_2F_1$  is hypergeometric function,  $\alpha$  is fractal dimension for a spherical nanocrystal  $\alpha = 0.33$ ,  $N(0)$  is initial concentration of monomers;  $N_E$  is final equilibrium concentration of monomers;  $N_C$  is concentration of nucleation centers, which is considered constant in this model.

For equation (5), one can obtain approximations for the initial ( $t \rightarrow 0$ ) (6) and final ( $t \rightarrow \infty$ ) (7) stages of the nanocrystal growth kinetics:

$$\frac{N(t) - N_e}{N(0) - N_e} = \exp\left\{-N_C \{(1 - \alpha)[N(0) - N_e]^\alpha k_D t\}^{\frac{1}{1-\alpha}}\right\}, \quad (6)$$

$$N(t) - N_e = A \exp\left\{-N_C^{1-\alpha} [N(0) + mN_C - N_e]^\alpha k_D t\right\}. \quad (7)$$

In both cases, the temperature dependence of the exponent is determined by the diffusion coefficient of the

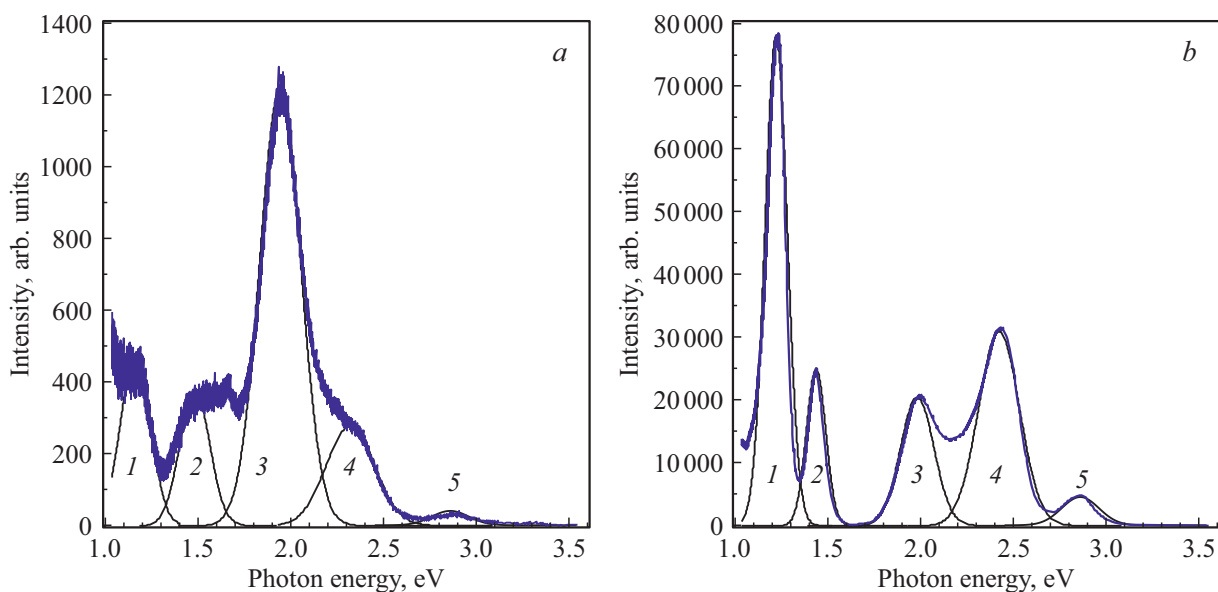


**Figure 6.** Photoluminescence spectra of titanium oxide samples immediately after synthesis (*a*) and after annealing in oxygen atmosphere at 900°C for 1 h (*b*). The experimental results are shown as an envelope curve, the results of separation using the Gaussian function are shown as numbered curves. The parameters of the emission bands are shown in the Table. The spectrum was divided into separate peaks using the Gaussian distribution. The parameters of separation are shown in the Table.

monomer, namely, of oxygen vacancy. The experimental results in Fig. 6 show that the energy of the crystallization process is of about 0.6 eV. A theoretical calculation shows that this energy shall determine the diffusion of the oxygen vacancy. The authors of the paper [28] estimated the activation energy of diffusion of oxygen vacancies from the surface (101) of a titanium oxide crystal and obtained a value ranging from 0.6 to 1.2 eV. The value of the activation energy obtained by us in this work is consistent with this value. The higher the partial pressure of oxygen and the lower the partial pressure of titanium are, the higher the concentration of crystallization centers in the film is. At large number of them, a large number of defects is formed in the matrix, which should contribute to the diffusion acceleration. In this regard, the diffusion coefficient may have a value less than the calculated value [28], which was calculated for single crystals. Accordingly, the value of the activation energy for the diffusion of oxygen vacancies over the film can be at the lower limit of the calculation, as was found experimentally in our case. This ensures the supposition that the main mechanism for the nanocrystalline formations increasing in thin films of titanium oxide is their compaction due to the escape of oxygen vacancies on the surface of growing nanocrystals. In this case, annealing causes the formation of large nanocrystals with pronounced boundaries. The boundaries between single crystals are well observed experimentally. The example is Fig. 1, which shows the size increasing of nanocrystals on the film surface with annealing time increasing.

Formulas (6) and (7) show that the formation of nanocrystals is affected by both temperature (due to

the temperature dependence of the diffusion coefficient of oxygen vacancies) and the initial concentration of crystallization centers. This value depends on the partial pressures of oxygen and titanium. These experimental facts confirm that the theoretical model developed by us agrees satisfactorily with the experimental results.

## Conclusion

After synthesizing the titanium oxide film by magnetron sputtering at partial pressure of oxygen in a reactor of 0.48 mTorr, it consists of small nanocrystals with sizes less than 5 nm. Annealing of films in the oxygen atmosphere at high temperatures causes oxygen vacancies to escape to the surface of the growing nanocrystal, which is enriched in interstitial titanium ions  $Ti^{+3}$ . These ions react with oxygen, and nanocrystals grow. The film is gradually densified, the nanocrystals increase in size due to the growth and merging of neighboring small nanocrystals into one larger nanocrystal. This process occurs with the activation energy of about 0.6 eV in the case of titanium oxide, which corresponds to the activation energy of the diffusion of the oxygen vacancy in titanium oxide. The experiments performed in this paper demonstrate the refraction index increasing, which indicates film densification during annealing. The emission intensity of films upon photoluminescence excitation increases after annealing. The intensity of the emission bands varies differently. The largest increasing corresponds to the concentration increasing of  $Ti^{+3}$  ions on the surface of titanium oxide nanocrystals,

which agrees with the proposed model of their growth, which assumes that oxygen vacancies diffuse to the surface of nanocrystals, the surface is enriched with  $Ti^{+3}$  ions, where they react with oxygen, causing the nanocrystals size increasing, which causes the growth of nanocrystals. The concentration of oxygen vacancies on the surface decreases after annealing. Since the magnitude of the resistivity is determined by these defects, the resistance of the films increases. Films remain stable for extended time period.

## Funding

This work was supported by the Ministry of Science and Higher Education of the Russian Federation, project No. 0004-2019-0003. The investigations were performed in the Institute of Nanotechnology of Microelectronics of the Russian Academy of Sciences (INME RAS) using Large Scale Research Facility Complex for Heterogeneous Integration Technologies and Silicon + Carbon Nanotechnologies.

## Conflict of interest

The authors declare that they have no conflict of interest.

## References

- [1] *Obstarczyk A., Kaczmarek D., Wojcieszak D., Mazur M., Domaradzki J., Kotwica T., Pastuszek R., Schmeisser D., Mazur P., Kot M.T.* // *Materials & Design*. 2019. V. 175. P. 107822. doi 10.1016/j.matdes.2019.107822
- [2] *Jiang S.S., He G., Gao J., Xiao D.Q., Jin P., Li W.D., Lv J.G., Liu M., Liu Y.M., Sun Z.Q.* // *Ceramics International*. 2016. V. 42. N 10. P. 11640–11649. doi 10.1016/j.ceramint.2016.04.067
- [3] *Carpenter M.A., Mathur S., Kolmakov A.* *Metal Oxide Nanomaterials for Chemical Sensors*. NY: Springer, 2013.
- [4] *Avasthi S., McClain W.E., Man G., Kahn A., Schwartz J., Sturm J.C.* // *Appl. Phys. Lett.* 2013. V. 102. N 20. P. 203901. doi 10.1063/1.4803446
- [5] *Nagamatsu K.A., Avasthi S., Sahasrabudhe G., Man G., Jhaveri J., Berg A.H., Schwartz J., Kahn A., Wagner S., Sturm J.C.* // *Appl. Phys. Lett.* 2015. V. 106. N 12. P. 123906. doi 10.1063/1.4916540
- [6] *Wang X., Wu G., Zhou B., Shen J.* // *Materials (Basel, Switzerland)*. 2013. V. 6. N 7. P. 2819–2830. doi 10.3390/ma6072819
- [7] *Ju Y., Li L., Wu Z., Jiang Y.* // *Energy Procedia*. 2011. V. 12. P. 450–455. doi 10.1016/j.egypro.2011.10.060
- [8] *Hoskins B.D., Strukov D.B.* // *J. Vacuum Science & Technology A: Vacuum, Surfaces, and Films*. 2017. V. 35. N 2. P. 20606. doi 10.1116/1.4974140
- [9] *Dannenbergh R., Greene P.* // *Thin Solid Films*. 2000. V. 360. N 1–2. P. 122–127. doi 10.1016/S0040-6090(99)00938-4
- [10] *Shyjumon I., Gopinadhan M., Helm C.A., Smirnov B.M., Hippler R.* // *Thin Solid Films*. 2006. V. 500. N 1–2. P. 41–51. doi 10.1016/j.tsf.2005.11.006
- [11] *Deskins N.A., Du J., Rao P.* // *Phys. Chem. Chem. Phys.: PCCP*. 2017. V. 19. N 28. P. 18671–18684. doi 10.1039/c7cp02940c
- [12] *Sahbeni K., Sta I., Jlassi M., Kandyla M., Hajji M., Kompitsas M., Dimassi W.* // *J. Phys. Chem. & Biophys.* 2017. V. 7. N 03. doi 10.4172/2161-0398.1000257
- [13] *Chen H.-C., Lee K.-S., Lee C.-C.* // *Appl. Opt.* 2008. V. 47. N 13. P. 284–7. doi 10.1364/AO.47.00C284
- [14] *Gallart M., Cottineau T., Hönerlage B., Keller V., Keller N., Gilliot P.* // *J. Appl. Phys.* 2018. V. 124. N 13. P. 133104. doi 10.1063/1.5043144
- [15] *Bulyarskiy S.V., Gorelik V.S., Gusarov G.G., Koiva D.A., Lakalin A.V.* // *Opt. Spectrosc.* 2020. V. 128. N 5. P. 590–595. doi 10.1134/S0030400X20050057
- [16] *Zhao J., Jia C., Duan H., Li H., Xie E.* // *J. Alloys Compd.* 2008. V. 461. N 1–2. P. 447–450. doi 10.1016/j.jallcom.2007.07.018
- [17] *Stevanovic A., Büttner M., Zhang Z., Yates J.T.* // *J. American Chem. Soc.* 2012. V. 134. N 1. P. 324–332. doi 10.1021/ja2072737
- [18] *Precltková J., Galář P., Trojánek F., Daniš S., Rezek B., Gregora I., Němcová Y., Malý P.* // *J. Appl. Phys.* 2010. V. 108. N 11. P. 113502. doi 10.1063/1.3512982
- [19] *Knorr F.J., Mercado C.C., McHale J.L.* // *J. Phys. Chem. C*. 2008. V. 112. N 33. P. 12786–12794. doi 10.1021/jp8039934
- [20] *Wang X., Feng Z., Shi J., Jia G., Shen S., Zhou J., Li C.* // *Phys. Chem. Chem. Phys.: PCCP*. 2010. V. 12. N 26. P. 7083–7090. doi 10.1039/b925277k
- [21] *Mercado C.C., Knorr F.J., McHale J.L.* // *ACS Nano*. 2012. V. 6. N 8. P. 7270–7280. doi 10.1021/nn302392p
- [22] *Mercado C., Seeley Z., Bandyopadhyay A., Bose S., McHale J.L.* // *ACS Appl. Mater. & Interfaces*. 2011. V. 3. N 7. P. 2281–2288. doi 10.1021/am2006433
- [23] *Santara B., Giri P.K., Imakita K., Fujii M.* // *J. Phys. Chem. C*. 2013. V. 117. N 44. P. 23402–23411. doi 10.1021/jp408249q
- [24] *Henderson M.A.* // *Surface Science*. 1995. V. 343. N 1–2. P. L1156–L1160. doi 10.1016/0039-6028(95)00849-7
- [25] *Bulyarskiy S.V., Svetukhin V.V.* // *J. Nanoparticle Research*. 2020. V. 22. N 12. doi 10.1007/s11051-020-05069-1
- [26] *Bulyarskiy S.V., Svetukhin V.V.* // *Silicon*. 2020. V. 13. P. 3321–3327. doi 10.1007/s12633-020-00703-y
- [27] *Johnson W.L., Sankey O.F., Dow J.D.* // *Phys. Rev. B*. 1984. V. 30. N 4. P. 2070–2073. doi 10.1103/PhysRevB.30.2070
- [28] *Scheiber P., Fidler M., Dulub O., Schmid M., Diebold U., Hou W., Aschauer U., Selloni A.* // *Phys. Rev. Lett.* 2012. V. 109. N 13. P. 136103. doi 10.1103/PhysRevLett.109.136103